Parkinson disease-associated mutation R1441H in LRRK2 prolongs the "active state" of its GTPase domain

Jingling Liao[a,b], Chun-Xiang Wu[a,b], Christopher Burlak[c], Sheng Zhang[a], Heather Sahm[a], Mu Wang[a], Zhong-Yin Zhang[a], Kurt W. Vogel[d], Mark Federici[d], Steve M. Riddle[d], R. Jeremy Nichols[e], Dali Liu[f], Mark R. Cookson[g], Todd A. Stone[h], and Quyen Q. Hoang[a,b,1]

[a]Department of Biochemistry and Molecular Biology and [b]Stark Neurosciences Institute, Indiana University School of Medicine, Indianapolis, IN 46202; [c]Department of Surgery, Indiana University School of Medicine, Indianapolis, IN 46202; [d]Thermo Fisher Scientific, Madison, WI 53719; [e]The Parkinson's Institute and Clinical Center, Sunnyvale, CA 94085; [f]Loyola University Chicago, Chicago, IL 60626; [g]Laboratory of Neurogenetics, National Institutes of Health, Bethesda, MD 20892; and [h]Department of Molecular and Cellular Biochemistry, Indiana University, Bloomington, IN 47405

Edited by Gregory A. Petsko, Weill Cornell Medical College, New York, NY, and approved February 6, 2014 (received for review December 16, 2013)

Mutation in leucine-rich-repeat kinase 2 (LRRK2) is a common cause of Parkinson disease (PD). A disease-causing point mutation R1441H/G/C in the GTPase domain of LRRK2 leads to overactivation of its kinase domain. However, the mechanism by which this mutation alters the normal function of its GTPase domain [Ras of complex proteins (Roc)] remains unclear. Here, we report the effects of R1441H mutation (Roc_{R1441H}) on the structure and activity of Roc. We show that Roc forms a stable monomeric conformation in solution that is catalytically active, thus demonstrating that LRRK2 is a bona fide self-contained GTPase. We further show that the R1441H mutation causes a twofold reduction in GTPase activity without affecting the structure, thermal stability, and GDP-binding affinity of Roc. However, the mutation causes a twofold increase in GTP-binding affinity of Roc, thus suggesting that the PD-causing mutation R1441H traps Roc in a more persistently activated state by increasing its affinity for GTP and, at the same time, compromising its GTP hydrolysis.

neurodegenerative disease | dimer | monomer | oligomeric states

Mutation in leucine-rich-repeat kinase 2 (LRRK2) is a common cause of Parkinson disease (PD) (1–5). LRRK2 is a large (2,527-aa) multidomain protein consisting of seven putative domains (2), including a Ras-like GTPase domain called Ras of complex proteins (Roc), followed by a domain called C-terminal of Roc (COR), which is then followed by a kinase domain (Kin). It remains unclear how perturbations of these activities result in disease; however, the most common mutation in LRRK2-associated PD, G2019S in the kinase domain, shows higher kinase activity than wild type; therefore, its overactivation might be associated with disease pathogenesis (6).

The tandem Roc-COR-Kin arrangement suggests that their activities might be coupled such that the GTPase activity of Roc might modulate the kinase activity. Indeed, several studies have shown that GTP binding to the Roc domain regulates the activity of the Kin domain (7, 8). Moreover, a PD-associated mutation in the Roc domain (R1441C) has been shown to have higher kinase activity (9), thus suggesting that mutations in the Roc domain, also up-regulate kinase activity.

Understanding the function of Roc and its mechanism of action is important for understanding the mechanism of PD pathogenesis and therapeutic development. However, because of the lack sufficient quantity of protein samples amendable for detailed investigations, the biochemical properties and enzymatic activities of the Roc domain of LRRK2 are poorly understood.

Here, we describe a stably folded construct of human Roc domain that enabled us to investigate quantitatively its biochemical and enzymatic properties. The results revealed that a PD-causing mutation R1441H in the Roc domain renders it less active at hydrolyzing GTP, as well as having higher affinity for GTP, than its wild-type counterpart, thereby increasing the residence time of its GTP-bound "active state," which is associated with PD pathogenesis (8).

Results and Discussion

Construction of a Stable Human LRRK2 Roc Domain. A construct of the Roc domain of LRRK2 has been previously reported to form a constitutive domain-swapped dimer (10). However, this is currently controversial because of the unusual domain-swap conformation and that such a dimer has not been demonstrated in solution. It has been suggested that the domain-swapped human Roc structure might have been an artifact of crystallization (11); however, we felt that this unusual structure might have been caused by the short flanking boundaries of the construct (residues 1333–1516). To design longer Roc constructs with extended N and C termini, we superimposed the human Roc structure [Protein Data Bank (PDB) ID code 3D6T] with an orthologous *Chlorobium tepidum* Roc-Cor structure (PDB ID code 3DPU) for comparisons. The most significant difference between the two structures is the topologies of the N terminus relative to the C terminus in each structure. In the human structure, the N terminus Cα is ∼33.6 Å from the C terminus and pointing away from each other (Fig. S1*A*). In contrast, in the *C. tepidum* structure, the N and C termini are closely packed together (Cα-Cα distance of ∼5.5 Å) via backbone H bonding that forms a small hydrophobic patch (Fig. S1*B*).

Significance

Mutations in the gene encoding for leucine-rich-repeat kinase 2 (LRRK2) are a common cause of Parkinson disease (PD). To understand how LRRK2 causes PD, we need to understand its normal functions and how they are altered by disease-causing mutations. This effort has been hampered by the lack of appropriate samples, which led to some confusion in the field. This study shows the construction of a stably folded domain of LRRK2 called Ras of complex proteins (Roc). We use the study to resolve two conflicting models of Roc oligomerization by quantitatively demonstrating its GTPase activity in both monomeric and dimeric states. We further show that a PD-causing mutation affects both GTP binding and GTPase activity of Roc.

Author contributions: Q.Q.H. designed research; J.L., C.-X.W., C.B., S.Z., H.S., M.W., and T.A.S. performed research; K.W.V., M.F., S.M.R., R.J.N., and M.R.C. contributed new reagents/analytic tools; J.L., Z.-Y.Z., D.L., and Q.Q.H. analyzed data; and J.L. and Q.Q.H. wrote the paper.

The authors declare no conflict of interest.

This article is a PNAS Direct Submission.

[1]To whom correspondence should be addressed. E-mail: qqhoang@iu.edu.

This article contains supporting information online at www.pnas.org/lookup/suppl/doi:10.1073/pnas.1323285111/-/DCSupplemental.

To determine whether this contact patch occurs in human LRRK2, we built a homology model of human Roc domain with extended termini spanning the residues predicted to be in the hydrophobic patch. Our homology model revealed a similar hydrophobic patch that consists of two contiguous segments, residues 1329–1332 and 1518–1524, at the N- and C-terminal extensions, respectively (Fig. 1). Visually, this patch appears to act as the "glue" that bonds the N- and C-terminal extensions together and would prevent a domain-swapped dimer from occurring. To investigate whether the patch affects the structure of Roc, we made a series of human Roc constructs with the N and C termini extending into the hydrophobic patch. A resulting construct consisting of residues 1329–1520 was highly stable and amendable for biochemical and biophysical experimentations.

Roc Domain Forms Stable Monomers. We expressed our terminal-extended Roc construct (Roc_{ext}) in *Escherichia coli* and purified it by sequentially passing it through a column containing Nickel-nitrilotriacetic acid (Ni-NTA), followed by size-exclusion chromatography. During the final step of purification, we noticed that Roc_{ext} eluted from the Superdex 200 column in two separate peaks (Fig. 2*A*). The first peak (at 91.8 mL) corresponded to a molecular mass of about 48 kDa (Roc_{48}), and the second peak (at 98.7 mL) corresponded to about 24 kDa (Roc_{24}) based on column calibration standard curve using the manufacturer's molecular mass standard kit. The theoretical mass of Roc_{ext} is 23.5 kDa, so Roc_{24} and Roc_{48} appear to represent the monomeric and dimeric conformations of Roc_{ext}, respectively. Consistent with this, Roc_{24} and Roc_{48} resolved identically on reducing SDS/PAGE with an apparent molecular mass of ~24 kDa, and they both reacted with antibodies against LRRK2 on Western blots (Fig. 2 *B* and *C*).

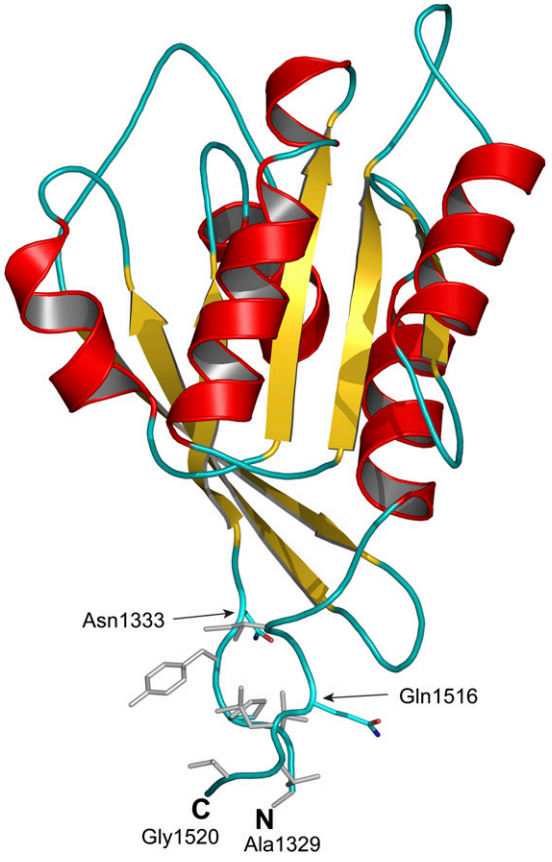

Fig. 1. Cartoon model of extended GTPase domain (Roc_{ext}). Shown is a homology model of our GTPase domain spanning residues 1329–1520 built based on the structure of bacterial Roc-Cor structure (PDB ID code 3DPU). The N and C terminals are labeled N and C, respectively. Arrows indicate the locations of terminals of previously determined structure of human GTPase domain (PDB ID code 3D6T). Colored gray are hydrophobic residues that form a hydrophobic patch gluing N and C terminal together.

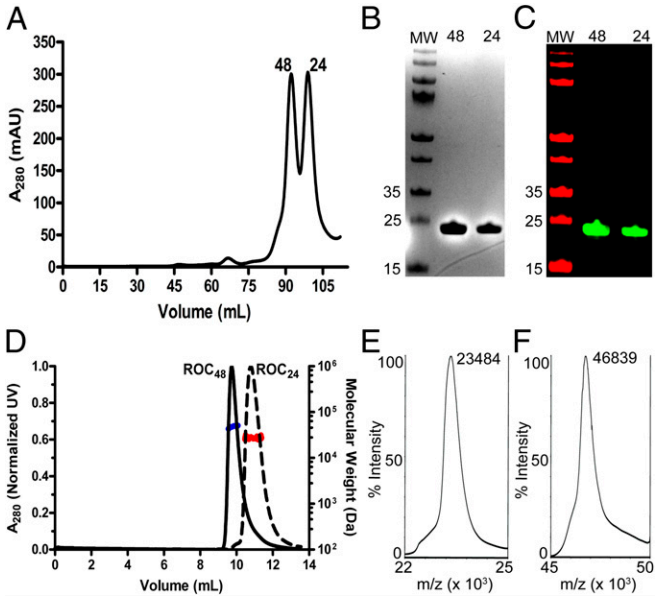

Fig. 2. Oligomeric states of Roc_{ext} in solution. (*A*) Size-exclusion chromatography elution profile of purified Roc_{ext} showing two peaks (48 and 24) that correspond to molecular masses of ~48 and ~24 kDa, respectively, based on standard calibration curve. (*B*) SDS/PAGE of peaks from *A*, 48 and 24. Molecular mass standards are labeled in kilodaltons to the left of the marker lane (MW). (*C*) Western blot of peaks from *A*, 48 and 24. Molecular mass standards are labeled in kilodaltons to the left of the marker lane (MW). (*D*) SEC-MALS profile of purified Roc_{ext} showing two peaks [48 (black solid line) and 24 (black dashed line)], along with their average molecular mass calculated from light scattering (blue and red lines, respectively). (*E* and *F*) MALDI-TOF MS spectra of 48 and 24, respectively.

To further authenticate our construct and to determine their precise molecular masses, we used matrix-assisted laser desorption/ionization time of flight (MALDI-TOF) mass spectrometry (MS). We detected a single mass of 23,484 Da in the Roc_{24} sample and 46,839 Da in the Roc_{48} sample, which correspond to the molecular masses of monomeric and dimeric forms of Roc_{ext}, respectively (Fig. 2 *E* and *F*).

To further confirm that the molecular masses determined by MS occur in solution, we used multiangle light scattering coupled with size-exclusion chromatography (SEC-MALS) to determine the molecular masses of Roc_{24} and Roc_{48} in solution. Roc_{24} resolved on SEC-MALS as a single peak with a calculated molecular mass of 25 ± 2 kDa, whereas Roc_{48} resolved as a single peak with a molecular mass of 46 ± 2 kDa, again consistent with the molecular mass of Roc_{ext} monomer and dimer within instrumental errors (Fig. 2*D*). These results confirm the existence of monomeric and dimeric Roc_{ext} in solution in the absence of a Cor domain.

The existence of Roc_{ext} as both dimers and monomers in solution indicate that it does not form constitutive dimer as previously suggested (10, 11). This gives rise to the possibility of a dynamic nucleotide-dependent dimerization as a regulation mechanism of Roc activity suggested by Gotthardt et al. (11). To investigate this possibility, we determined whether Roc_{48} changes its conformation upon binding to guanine nucleotides by incubating Roc_{48} with GDP or GppNHp for 2 h using standard nucleotide-exchange procedures (12). As shown in Fig. 3*A*, virtually all of Roc_{48} was converted to Roc_{24} upon binding either GDP or

GppNHp. We again used SEC-MALS to confirm that this is a bona fide conversion of dimers into monomers (Fig. 3*B*).

At the onset, we anticipated that dimer–monomer equilibrium might be regulated by GTP/GDP cycling; however, this was not the case because we found that GDP and GTP analog both converted the dimers into monomers with equal potency. Moreover, the physiological concentrations of guanine nucleotides (~500 μM GTP and ~50 μM GDP) are higher than needed for the conversion, which would render Roc_{ext} mostly monomeric; therefore, the observed dimer–monomer conversion of Roc_{ext} is unlikely to be physiologically relevant. For this reason, our focus turned to understanding the structure and function of the monomeric Roc_{24}.

Monomeric Roc_{24} Is Catalytically Active. The literature currently suggests that dimerization of Roc is required for its GTPase activity (10, 11), but this requirement is uncertain because one of the two structures that provided this insight showed an unusual domain-swapped conformation not seen in other GTPases, whereas the second structure required intermolecular exchange of an arginine residue in *trans* to constitute an active site, but the required arginine does not exist in human LRRK2 (11). Having created a stable monomeric Roc construct enabled us to test these requirements. First, we set out to determine whether Roc_{24} has the ability to hydrolyze GTP to generate GDP by using normal-phase hydrophilic interaction liquid chromatography (HILIC) HPLC coupled to electrospray mass-spectrometry (LC/MS). GTP and GDP resolved as two well separated peaks with determined molecular mass of 524 and 444 Da, which correspond to the theoretical molecular mass of GTP (523 Da) and GDP (443 Da), respectively (Fig. S2). As shown in Fig. 4*A*, the production of GDP increased in a concentration-dependent manner, thus indicating that GTP was being converted to GDP.

To understand the GTPase activity of Roc_{24} in more detail, we determined its steady-state kinetic parameters using the EnzCheck assay kit (Molecular Probes). Initial velocities were measured as a function of GTP concentrations. The resulting saturation curve adheres to the simple Michaelis–Menten equation, which allowed us to calculate the steady-state kinetic parameters by nonlinear least-squares fit using the software Prism6 (GraphPad). As summarized in Fig. 4*B*, $k_{cat} = 0.020 \pm 0.001$ min^{-1} and $K_m = 553 \pm 94$ μM. The low turnover rate and high K_m indicate that isolated Roc_{ext} is a slow enzyme and suggest that it might require activating and/or exchanging factors to efficiently hydrolyze GTP.

G proteins that cycle between GTP-bound (active) and GDP-bound (inactive) states as a switching mechanism commonly have low intrinsic GTPase activity. Ras, for example, has equally low intrinsic GTPase activity ($k_{cat} = 0.028$ min^{-1}) (13). The conversion between GDP and GTP by Ras family GTPases is usually accelerated by guanine nucleotide exchange factors (GEFs), GTPase activating proteins (GAPs), or oligomerization-induced conformational

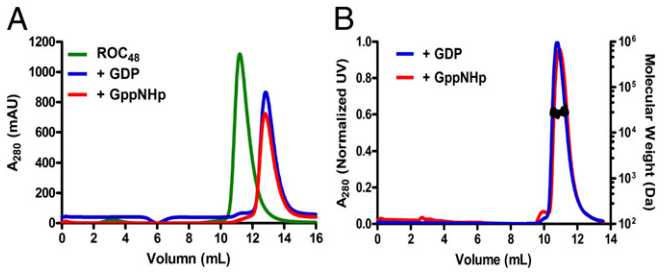

Fig. 3. Conversion of Roc_{48} to monomers upon guanine nucleotide binding. (*A*) Size-exclusion chromatography profile of Roc_{48} apo state (green, ~48 kDa), GDP-bound (blue, ~24 kDa), and GppNHp-bound (red, ~24 kDa) shows conversion of the Roc_{48} peak into Roc_{24} peaks upon binding to either GDP or GTP. (*B*) SEC-MALS profile of GDP- and GppNHp-bound Roc_{ext} with calculated molecular masses of 25 kDa for both (black line on the peak).

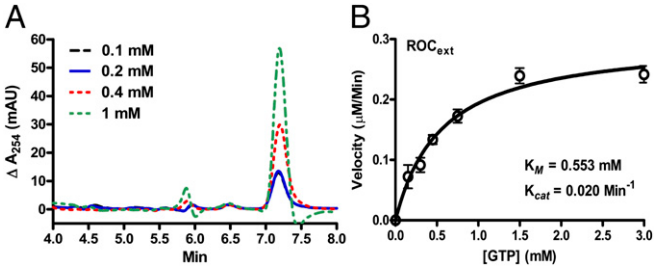

Fig. 4. GTPase activity of Roc_{ext}. (*A*) Background-subtracted LC/MS spectra of GDP generated by Roc_{ext} GTP hydrolysis activity. Reaction was conducted with a range of GTP concentrations (0.1–1 mM). This graph shows proportional production of GDP with respect to the concentration of GTP. (*B*) Steady-state kinetics of Roc_{ext} GTP hydrolysis. Data (open circles) is an average of three independent measurements with error bars (± SEM) indicated.

changes (14, 15). The low k_{cat} observed for Roc_{ext} is in line with the intrinsic activity of this family of enzymes; however, strong activating or exchange factors of LRRK2 have not yet been identified.

The Michaelis constant K_m (which is defined as the rate of dissociation of the enzyme–substrate complex [ES] k_{-1} plus the rate of forming the product and free enzyme [P and E] k_{+2} divided by the rate of substrate binding to enzyme forming [ES] k_{+1}; $K_m = (k_{+2} + k_{-1})/k_{+1}$) is commonly used to approximate the affinity of the substrate with the enzyme K_d (defined as [E][S]/[ES]). When the chemical process is fast, the K_m approximates K_d. However, GTPases are usually slow at hydrolyzing its substrate (represented by the rate constant k_{+2}) and commonly bind their product GDP with higher affinity than their substrate GTP. This results in slow dissociation of the enzyme–product complex [EP] and renders the K_m unrepresentative of the K_d for GTP. To estimate the affinity of Roc_{ext} for GTP, we determined the K_d of Roc_{ext} for GTP nonhydrolyzable analog GTPγS using a fluorescence polarization (FP) assay (16, 17). As shown in Fig. 5*A*, the dissociation constant (K_d) of BODIBY-FL-GTPγS is 7.85 μM, which is two orders of magnitude lower than the K_m, thus confirming that the K_m does not represent K_d in this case. Note that we used BODIBY-FL-GTPγS instead of GTP to avoid complications associated with GTP hydrolysis during the binding assay as commonly used in the field. Although the FP assay that we used is well established, to confirm that the binding of BODIBY-FL-GTPγS is an appropriate approximation of GTP binding, we titrated Roc_{ext} prebound with BODIPY-FL-GTPγS with unlabeled natural GTP. We found that GTP effectively displaced BODIPY-FL-GTPγS (Fig. 5*B*), thus confirming that BODIPY-FL-GTPγS binds to the same site as natural GTP on Roc_{ext}.

The affinity of Roc_{ext} with GTP in the low-micromolar range is relatively weak compared with typical small GTPases (which are in the sub-nanomolar range), but it is similar to that of large GTPase dynamin family (which are in micromolar range) (18). The weak affinity of Roc_{ext} for nucleotide and the relatively small difference in its affinity for GTP vs. GDP (7.85 vs. 0.47 μM) suggests that it might not require GEFs for nucleotide-exchange cycling (physiological concentrations of GTP and GDP are ~500 and ~50 μM, respectively) (19). However, its low turnover rate of 0.02 molecules per minute suggests that it could require an activation factor for efficient hydrolysis of GTP, as observed in other GTPases.

Conformations of GDP- and GppNHp-Bound Roc. GTPases typically function as molecular switches that toggle on/off by undergoing conformational changes upon binding GTP and GDP. Thus, by analogy, the Roc domain of LRRK2 is believed to regulate its kinase domain via a similar mechanism. To investigate this, we characterized the structure of Roc_{ext} by using circular dichroism

BIOCHEMISTRY

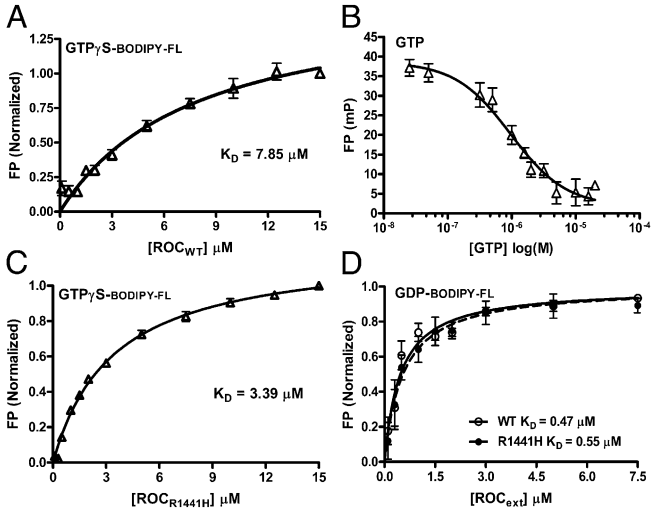

Fig. 5. Guanine nucleotide-binding affinity. (*A*) BODIPY-FL-GTPγS–binding affinity to Roc_{WT} was measured using FP assay. Data represented an average of triplicates with error bars (SEM) shown. The dissociation constant (K_D) was determined by fitting nonlinear curve regression using GraphPad Prism 6. (*B*) Competition of prebound BODIPY-labeled GTPγS titrated with natural unlabeled GTP showed that the BODIPY-labeled nucleotide binds to the same site on Roc_{WT} as natural nucleotide. (*C*) BODIPY-FL- GTPγS–binding affinity to Roc_{R1441H} was measured using FP assay. Data represented an average of triplicates with error bars (SEM) shown. The dissociation constant was determined as above. (*D*) BODIPY-FL-GDP–binding affinity to Roc_{WT} and Roc_{R1441H} was measured using FP assay, and the dissociation constant was determined as above.

(CD) spectroscopy to determine the secondary structure contents of Roc_{ext} bound with GDP and GppNHp (nucleotide free Roc_{ext} is not stable and therefore was not characterized). We observed only small structural differences between the two forms, which are composed of 41% and 46% α-helix in its GDP- and GppNHp-bound forms, respectively (Fig. 6*A*). This result suggests that the switching mechanism does not involve large structural changes. This is consistent with other small GTPase where GDP/GTP cycling typically causes conformational changes in two small loop regions, known as switch 1 and switch 2 (20, 21). However, in large GTPases, the small conformational changes in the switch regions lead to large global structural rearrangements. For example, GTP hydrolysis by the GTPase domain of dynamin1 causes large conformational changes to helical domains in its N and C termini (called N_{GTPase} and C_{GTPase}) to provide the mechanical forces necessary for pinching off invaginated coated pits (22, 23). Interestingly, our homology model of LRRK2 also shows flanking structures similar to N_{GTPase} and C_{GTPase}, which suggests that the GTPase domain of LRRK2 could potentially function in a similar manner.

Roc Carrying PD Mutation Has Lower GTPase Activity than Wild Type. After establishing that the Roc domain of LRRK2 is as a bona fide self-contained GTPase, we turned our focus to investigate how the PD-causing mutation in Roc R1441H (Roc_{R1441H}) affects its properties. We introduced the mutation by using PCR-based site-directed mutagenesis using our Roc_{ext} DNA template and confirmed by DNA sequencing. Protein expression and purification procedures are as described for Roc_{ext} above. The mutated amino acid sequence was authenticated by mass spectrometry (Fig. S3).

We determined the GTPase activity of Roc_{R1441H} using the same EnzCheck assay described above and compared it to wild-type Roc_{ext}. We found that Roc_{R1441H} showed significantly lower activity than Roc_{ext} (Fig. 7*A*), suggesting that the point mutation does indeed change the GTPase activity of LRRK2 and might constitute a basis for PD pathogenesis. This is consistent with previously reported observations of two other amino acid substitutions at 1441 (R1441C and R1441G) using proteins pulled down from rat brains (24).

To investigate the GTPase activity of Roc_{R1441H} in more detail, we determined its enzyme kinetics. We found that it is more than twofold less active than Roc_{ext} with k_{cat} = 0.009 vs. 0.020 min^{-1}, respectively, with $K_m = 112 \pm 22$ μM (Fig. 7*B*), suggesting that the point-mutation R1441H affects both GTP-binding affinity, as well as its biochemical hydrolysis, which would undoubtedly trap Roc in a more persistent active state. GTP-bound state of Roc has been shown to activate kinase activity of LRRK2, which is associated with PD pathogenesis (8, 25).

Roc_{R1441H} Has Higher Affinity for GTP than Wild Type. To understand how the R1441H mutation led to a reduction in GTPase activity of Roc, we performed a battery of biochemical assays to examine its effects on structural features, thermal stability, and guanine nucleotide-binding affinity. We found that the point mutation dose not affect the structure or thermal stability of Roc (Figs. 6*B* and 8*A*), thus suggesting that the reduction in GTPase activity of the mutant might be caused by biochemical perturbations as opposed to structural.

When we compared guanine nucleotide-binding affinity of Roc_{R1441H} with Roc_{ext} using a fluorescence polarization assays as described above, we found no significant difference in their affinity for GDP (Fig. 5*D*). However, the GTPγS-binding affinity of Roc_{R1414H} is twofold higher than that of Roc_{ext}, K_d = 3.39 vs. 7.85 μM, respectively (Fig. 5*C*). This seems counterintuitive because higher substrate affinity usually results in higher activity instead of lower as we observed.

To confirm the observed difference in GTP-binding affinity, we determined the thermal denaturation of Roc_{ext} and Roc_{R1441H} bound with GDP and GppNHp using differential scanning fluorimetry (26). We found no significant difference in the denaturation curve between GDP-bound Roc_{R1441H} and Roc_{ext}, which is consistent with their similar affinities for GDP (Fig. 8*B*). However, GppNHp-bound Roc_{R1441H} has a melting temperature (Tm) ~3.1 °C higher than Roc_{ext}, thus confirming the above observation that the R1441H mutation does indeed lead to increased GTP-binding affinity. More importantly, the observed increase in GTP-binding affinity and decreased in GTPase activity would independently result in a prolonged active state of Roc, having both features in a single mutation is a "double-whammy" that together would trap Roc in a more persistent active state.

Conclusions

Over the past 10 y, the field has been pursuing disparately to understand the functions of LRRK2 and how it is affected by

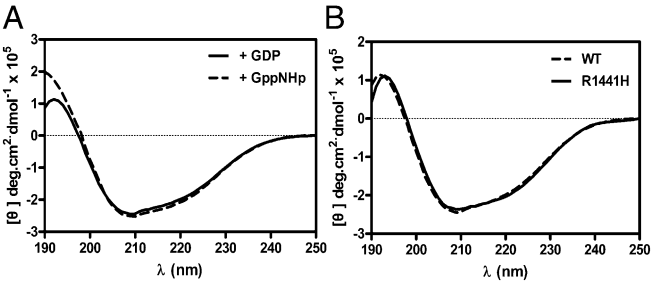

Fig. 6. Structure characteristic of Roc_{WT} and Roc_{R1441H}. (*A*) CD spectra of Roc_{WT} bound to GDP (solid line) or GppNHp (dashed line) showed no significant difference between two forms. (*B*) CD spectra of Roc_{R1441H} (solid line) and Roc_{WT} (dashed line) showed no significant difference between them.

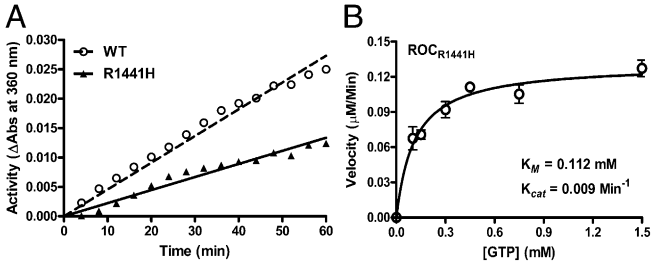

Fig. 7. GTPase activity of Roc$_{R1441H}$. (*A*) Time course (1 h) GTPase activity assayed showing Roc$_{R1441H}$ (filled triangle with solid line) is less active than Roc$_{WT}$ (open circle with dashed line). (*B*) Steady-state kinetics of Roc$_{R1441H}$ GTP hydrolysis confirming that Roc$_{R1441H}$ has a lower activity than Roc$_{WT}$. Data (open circle) are averages of three independent measurements with error bars (SEM) indicated.

PD-associated mutations. A major hurdle in the field has been the difficulty in obtaining sufficient quantity and quality of samples (both full-length and individual domains) suitable for quantitative investigations. We have produced a suitable Roc domain of LRRK2 that enabled us to quantitatively demonstrate that the Roc domain of LRRK2 is a bona fide GTPase, which clarifies a current confusion in the field regarding the necessity of dimerization for Roc activity. The kinase activity of LRRK2 has been shown to be overactivated in PD-associated R1441H mutant; here, we show that it traps Roc in a more persistently activated state by increasing its affinity for GTP and, at the same time, decreasing its GTPase activity, thus providing insights into the mutant's mechanism of PD pathogenesis.

Methods

Homology Modeling. Homology models of human LRRK2 GTPase domain were built based on the structure of *C. tepidum* Roco (PDB ID code 3DPU) by using the program Modeler 9.12 (Andrej Sali, University of California, San Francisco, CA). Molecular graphics display and presentation were made using PyMol (www.pymol.org).

Protein Expression and Purification. An extended GTPase domain of LRRK2 consisting of residues 1329–1520 (Roc$_{ext}$) was subcloned into a pETDuet-1 vector (Novagen, Merck) using PCR cloning techniques. The resulting protein consisting of an N-terminal hexahistidine tag was expressed from Rosetta2 (DE3) *E. coli* (Novagen) by inducing with 0.5 mM isopropyl-β-D-thiogalactopyranoside for 16 h at 20 °C. Cells harvested by centrifugation and lysed by sonication in buffer containing 10 mM Hepes (pH 7.4), 250 mM NaCl, 10 mM magnesium acetate (MgAc), 10 mM glycine, 20 mM imidazole, 10 μM GDP, and 5% (vol/vol) glycerol. Cell debris was cleared by ultracentrifugation at 35,000 rpm in a Beckman 70Ti rotor. The supernatant was incubated with Ni-NTA Agarose (Life Technologies) for 2 h at 4 °C, then washed with lysis buffer (detailed above), and eluted with buffer containing 10 mM Hepes (pH 7.4), 250 mM NaCl, 10 mM MgAc, 10 mM glycine, 300 mM imidazole, 1 mM DTT, 10 μM GDP, and 5% glycerol. The purified protein was then "polished" by passing through a size-exclusion column (Superdex 200; GE Healthcare) in buffer containing 10 mM Hepes (pH 7.4), 150 mM NaCl, 10 mM MgAc, 10 mM glycine, 1 mM DTT, and 5% glycerol. The purified protein was then concentrated to ~10 mg/mL, flash frozen in liquid nitrogen, and stored at −80 °C.

Western Blotting. A polyclonal antibody against the Roc domain of human LRRK2 (residues 1329–1520) was purchased from Cocalico Biologicals. A secondary antibody, IRDye 680RD Goat anti-rabbit, was purchased from LI-COR Biosciences. Roc$_{48}$ and Roc$_{24}$ were collected from Roc$_{48}$ peak and Roc$_{24}$ peak separately and loaded into SDS/PAGE. Protein bands were detected by the primary antibody and secondary antibody sequentially, and final membrane was scanned by using an ODYSSEY Infrared Imaging System (LI-COR Biosciences).

SEC-MALS. To determine the absolute molecular mass of Roc$_{ext}$ in solution, we used multiple angle light scattering. Our experimental setup includes an AKTA FPLC (GE Healthcare Biosciences) with a silica-based size-exclusion chromatography column (WTC-030S5; Wyatt Technology) as an LC unit. Down from the LC is a refractive index detector (Optilab T-rEX; Wyatt Technology), followed by a multiple light scattering detector (Dawn HeleosII; Wyatt Technology) for determining protein concentration and particle size, respectively. Each sample injection consisted of ~1 mg of purified Roc$_{ext}$ in buffer containing 10 mM Hepes (pH 7.4), 0.15 M NaCl, 10 mM MgAc, 10 mM glycine, 1 mM DTT, and 5% glycerol. Flow rate was set at 0.4 mL/min, and data were collected every 2-s interval. Data processing and analysis were performed using the ASTRA software (Wyatt Technology).

Mass Spectrometry. Molecular masses of Roc$_{48}$ and Roc$_{24}$ were determined using MALDI-TOF (AB Sciex). Protein samples were desalted by using ZipTip-C18 columns (EMD MILLIPORE) and eluted with acetonitrile; 1.5 μL of eluent was spotted on a stainless steel MALDI plate and allowed to dry. A "sandwich" of sample–matrix–sample was formed by layering 1.5 μL of matrix [sinapinic acid (stock, 10 mg/mL) in 75% acetonitrile and 0.1% TFA] on top of the dried protein sample spot, followed by another layer of protein sample on top of the dried matrix. Sample was analyzed using standard MALDI-TOF methods.

To determine GTPase activity of Roc$_{ext}$ by MS, we used normal-phase ZIC-HILIC (EMD Millipore) HPLC coupled to electrospray MS; 20 μM Roc$_{ext}$ was incubated with various concentration of GTP (0.1, 0.2, 0.4, and 1 mM) at 25 °C for 1 h. After incubation, protein samples were be denatured at 100 °C for 10 min, followed by centrifuging to remove denatured protein. Samples were loaded into ZIC-HILIC HPLC equilibrated in 90% acetonitrile and 30 mM ammonium acetate and eluted in 70% acetonitrile and 30 mM ammonium acetate isocratically. The eluted nucleotides molecular mass was determined by inline electrospray MS.

CD Spectroscopy. CD spectra were collected on a Biologic Science Instruments MOS450 AF/CD spectrometer with slit width of 1.0 mm and data acquisition of 1.0 s. The protein samples with concentrations ranging from 0.46 to 0.86 mg/mL (based on absorbance at 280 nm) were dissolved in the buffer containing 10 mM Tris·HCl (pH 7.4), 150 mM NaCl, 5 mM $MgCl_2$, 1 mM DTT, and 5% glycerol. The data used for graphical presentation and analyses were each an average of five different scans.

Fluorescence Polarization Nucleotide-Binding Assay. To estimate the binding affinity of guanine nucleotides, BODIPY-FL-GTPγS (100 nM) or 150 nM BODIPY-FL-GDP (150 nM) (Life Technologies) were titrated with Roc$_{ext}$ (starting at 0.1 μM) until saturation was reached (15 and 10 μM, respectively). Fluorescence polarization was read using an EnVison 2102 Multilabel Plate Reader (Perkin-Elmer) with excitation at 485 nm and emission at 535 nm. Experiments were performed at 25 °C in buffer 10 mM Hepes (pH 7.4), 150 mM NaCl, 10 mM MgAc, 10 mM glycine, 4 mM EDTA, 1 mM DTT, 5% glycerol. Data were analyzed using Prism 6 (GraphPad Software).

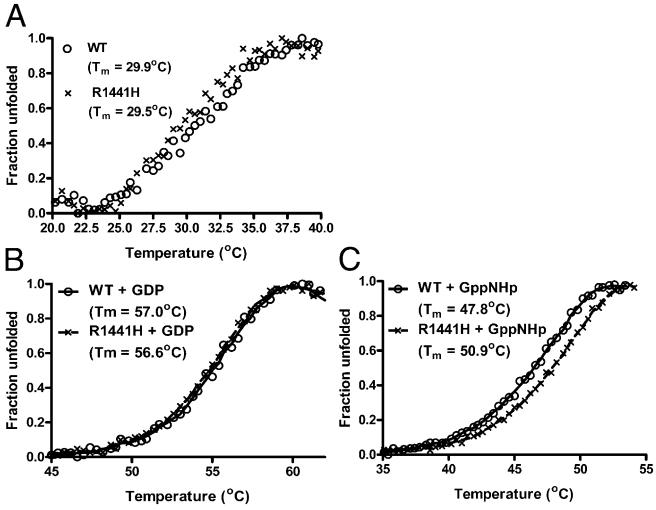

Fig. 8. Roc$_{WT}$ and Roc$_{R1441H}$ thermal stability determined by ThermoFluor assay. (*A*) Melting curve showing that Roc$_{WT}$ (opened circle) and Roc$_{R1441H}$ (X) have similar Tm values in nucleotide-free forms. (*B*) Melting curve of GDP-bound Roc$_{WT}$ and Roc$_{R1441H}$ showing similar thermal stability. (*C*) Melting curve of GppNHp-bound Roc showing that Roc$_{R1441H}$ is more thermally stable than Roc$_{WT}$, indicative of a higher affinity of Roc$_{R1441H}$ for GTP.

GTPase Activity Assay. GTPase activity of Roc_{ext} was assessed by using the Enzcheck assay kit (Life Technologies) according to manufacturer's instructions. Briefly, Roc_{ext} (15 μM) was incubated with different concentration of GTP (0.15, 0.3, 0.45, 0.75, 1.5, and 3 mM) in in buffer containing 10 mM Hepes, 150 mM NaCl, 10 mM $MgCl_2$, 1 mM DTT, and 5% glycerol at 25 °C. Absorbances at 360 nm were recorded every 4 min for a duration of 60 min using a microplate reader. The amount of inorganic phosphate released from GTP hydrolysis at each time point was determined by extrapolation using a phosphate standard curve. Kinetic parameters were determined by fitting the data to Michaelis–Menten equation using GraphPad Prism 6.

Fluorescence Polarization-Based Nucleotide Competition Assay. To ensure that the binding that we observed between GTP/GDP and Roc_{ext} was mediated by the nucleotides and not the BODIPY molecules attached to them, we performed nucleotide-competition assays for each nucleotide. Roc_{ext} (2 μM) was preincubated with 100 nM BODIPY-FL-GTPγS or 150 nM BODIPY-FL-GDP (Life Technologies) for 10 min at 25 °C in 384-wells black plate (NUNC). Then, the Roc_{ext}–BODIPY–nucleotide complex was titrated with unlabeled natural GTP or GDP (started at 25 nM) until the binding between Roc_{ext} and labeled nucleotide was inhibited completely (20 μM). The fluorescence polarization was read in an EnVison 2102 Multipliable Plate Reader (Perkin-Elmer) using excitation at 485 nm and emission at 535 nm. Experiments were performed at 25 °C in buffer containing 10 mM Hepes (pH 7.4), 150 mM NaCl, 10 mM MgAc, 10 mM glycine, 4 mM EDTA, 1 mM DTT, 5% glycerol. The titration plots were fitted in a nonlinear regression curve using GraphPad Prism 6.

ThermoFluor Assay. Solutions of 7.5 μL of 16× Sypro Orange (prepared from 5,000× stock concentrate; Life Technologies) in buffer containing 10 mM Hepes (pH 7.4), 0.15 M NaCl, 10 mM MgAc, 10 mM glycine, 1 mM DTT, and 5% glycerol, 12.5 μL of 4 mM GDP or GppNHp (Sigma), and 5 μL of 25 μM Roc_{ext} or Roc_{ext} R1441H were added to a 96-well thin-walled PCR plate. The plate was heated in the Real Time PCR Detection System (Mastercycler Realplex; Eppendorf) from 20 °C to 85 °C, and fluorescence was recorded in increments of 0.4 °C. The emission wavelength was set at 550 nm.

ACKNOWLEDGMENTS. We thank Clark Wells and Yuro Takagi for helpful discussions. Q.Q.H. acknowledges support from a Michael J. Fox Foundation Community Fast Track grant. Q.Q.H. acknowledges additional support from the Indiana University School of Medicine's Biomedical Research grant and the Showalter Research Trust grant. This research was supported, in part, by the Intramural Research Program of the National Institutes of Health, National Institute on Aging (M.R.C.). R.J.N. acknowledges the Brin/Wojcicki Foundation for support. S.Z. and Z.-Y.Z. were supported in part by Grant RO1 CA69202.

1. Cookson MR (2010) The role of leucine-rich repeat kinase 2 (LRRK2) in Parkinson's disease. *Nat Rev Neurosci* 11(12):791–797.
2. Mata IF, Wedemeyer WJ, Farrer MJ, Taylor JP, Gallo KA (2006) LRRK2 in Parkinson's disease: Protein domains and functional insights. *Trends Neurosci* 29(5):286–293.
3. Giasson BI, Van Deerlin VM (2008) Mutations in LRRK2 as a cause of Parkinson's disease. *Neurosignals* 16(1):99–105.
4. Zimprich A, et al. (2004) Mutations in LRRK2 cause autosomal-dominant parkinsonism with pleomorphic pathology. *Neuron* 44(4):601–607.
5. Paisán-Ruíz C, et al. (2004) Cloning of the gene containing mutations that cause PARK8-linked Parkinson's disease. *Neuron* 44(4):595–600.
6. Greggio E, et al. (2006) Kinase activity is required for the toxic effects of mutant LRRK2/dardarin. *Neurobiol Dis* 23(2):329–341.
7. Guo L, et al. (2007) The Parkinson's disease-associated protein, leucine-rich repeat kinase 2 (LRRK2), is an authentic GTPase that stimulates kinase activity. *Exp Cell Res* 313(16):3658–3670.
8. Ito G, et al. (2007) GTP binding is essential to the protein kinase activity of LRRK2, a causative gene product for familial Parkinson's disease. *Biochemistry* 46(5):1380–1388.
9. West AB, et al. (2005) Parkinson's disease-associated mutations in leucine-rich repeat kinase 2 augment kinase activity. *Proc Natl Acad Sci USA* 102(46):16842–16847.
10. Deng J, et al. (2008) Structure of the ROC domain from the Parkinson's disease-associated leucine-rich repeat kinase 2 reveals a dimeric GTPase. *Proc Natl Acad Sci USA* 105(5):1499–1504.
11. Gotthardt K, Weyand M, Kortholt A, Van Haastert PJ, Wittinghofer A (2008) Structure of the Roc-COR domain tandem of C. tepidum, a prokaryotic homologue of the human LRRK2 Parkinson kinase. *EMBO J* 27(16):2239–2249.
12. Wells C, Jiang X, Gutowski S, Sternweis PC (2002) Functional characterization of p115 RhoGEF. *Methods Enzymol* 345:371–382.
13. Spoerner M, et al. (2010) Conformational states of human rat sarcoma (Ras) protein complexed with its natural ligand GTP and their role for effector interaction and GTP hydrolysis. *J Biol Chem* 285(51):39768–39778.
14. Cherfils J, Zeghouf M (2011) Chronicles of the GTPase switch. *Nat Chem Biol* 7(8):493–495.
15. Cherfils J, Zeghouf M (2013) Regulation of small GTPases by GEFs, GAPs, and GDIs. *Physiol Rev* 93(1):269–309.
16. McEwen DP, Gee KR, Kang HC, Neubig RR (2002) Fluorescence approaches to study G protein mechanisms. *Methods Enzymol* 344:403–420.
17. McEwen DP, Gee KR, Kang HC, Neubig RR (2001) Fluorescent BODIPY-GTP analogs: Real-time measurement of nucleotide binding to G proteins. *Anal Biochem* 291(1):109–117.
18. Warnock DE, Schmid SL (1996) Dynamin GTPase, a force-generating molecular switch. *Bioessays* 18(11):885–893.
19. Traut TW (1994) Physiological concentrations of purines and pyrimidines. *Mol Cell Biochem* 140(1):1–22.
20. Pingoud A, et al. (1988) Spectroscopic and hydrodynamic studies reveal structural differences in normal and transforming H-ras gene products. *Biochemistry* 27(13):4735–4740.
21. Valencia A, Serrano L, Caballero R, Anderson PS, Lacal JC (1988) Conformational alterations detected by circular dichroism induced in the normal ras p21 protein by activating point mutations at position 12, 59, or 61. *Eur J Biochem* 174(4):621–627.
22. Faelber K, et al. (2011) Crystal structure of nucleotide-free dynamin. *Nature* 477(7366):556–560.
23. Ford MGJ, Jenni S, Nunnari J (2011) The crystal structure of dynamin. *Nature* 477(7366):561–566.
24. Li X, et al. (2007) Leucine-rich repeat kinase 2 (LRRK2)/PARK8 possesses GTPase activity that is altered in familial Parkinson's disease R1441C/G mutants. *J Neurochem* 103(1):238–247.
25. Smith WW, et al. (2006) Kinase activity of mutant LRRK2 mediates neuronal toxicity. *Nat Neurosci* 9(10):1231–1233.
26. Niesen FH, Berglund H, Vedadi M (2007) The use of differential scanning fluorimetry to detect ligand interactions that promote protein stability. *Nat Protoc* 2(9):2212–2221.